Journal of Molecular Liquids 349 (2022) 118097

Contents lists available at ScienceDirect

Journal of Molecular Liquids

journal homepage: www.elsevier.com/locate/molliq

Structure and local order of lyotropic cholesteric calamitic phases: The effect of the chiral molecule

O.R. Santos [a,*], D. Reis [b], A.G. Oliveira-Filho [b], C.L.P. Oliveira [b], A.M. Figueiredo Neto [b]

[a] Universidade Tecnológica Federal do Paraná, Campus Campo Mourão, 87301-006 Campo Mourão, Paraná, Brazil
[b] Universidade de São Paulo, São Paulo, Brazil

ARTICLE INFO

Article history:
Received 9 August 2021
Revised 29 October 2021
Accepted 10 November 2021
Available online 25 November 2021

Keywords:
Cholesteric liquid crystal
SAXS
Small-angle X-ray scattering
Pseudo-lamellar structure

ABSTRACT

We investigate a lyotropic mixture presenting in the calamitic nematic phase (N_C) and its corresponding calamitic cholesteric phase (Ch_C), where a small amount of the chiral agent (brucine sulfate) was added. Different experimental techniques (polarized optical microscopy and laser conoscopy) were used to characterize the phases. The main technique employed in the analysis of the structure and local ordering at nanoscale is the Small-Angle X-ray Scattering, where advanced modeling analysis were applied. The lyotropic nematic mixtures was composed of potassium laurate/potassium sulfate/dodecanol/water and the cholesteric phases were obtained from these mixtures, by adding the chiral molecule, brucine sulfate. From an advanced modeling analysis, we show that the micellar overall shape is not modified by the doping with brucine. However, the presence of the brucine between micelles in the Ch_C phase imposes a higher correlation between micelles along the direction of the pseudo-lamellar ordering. Finally, the order parameter $\langle P2 \rangle$ was calculated and these values for the phases N_C and Ch_C are 0.8133(6) and 0.747(2), respectively, indicating a slightly higher orientational ordering in the N_C phase.

1. Introduction

Lyotropic liquid crystals are mixtures of amphiphilic molecules and solvents (usually water) in suitable conditions of temperature, relative concentrations of the different compounds, and pressure [1]. The basic units of lyotropics are molecular aggregates (micelles) [2,3]. These materials may exhibit three different nematic phases: two uniaxial (calamitic - N_C and discotic - N_D) and one biaxial (N_B) [4–9].

Similarly to the lyotropic nematic phases, the lyotropic cholesteric, or chiral nematic phase, may be obtained by adding chiral molecules to lyotropic nematic mesophases or directly using L– or D-enantiomer of a racemic (DL-form) amphiphilic molecule [10–15]. Three different types of cholesteric phases have been identified [11,16–18]: calamitic cholesteric – Ch_C discotic cholesteric – Ch_D and biaxial cholesteric (Ch_B) [19]. Likewise to nematics, the concomitant presence of the three cholesteric phases happens only in mixtures with, at least, a surfactant and a co-surfactant. In cholesterics, micelles are organized in a helicoidal structure, characterized by a pitch (P) of the helix. This parameter depends on the concentration of the chiral dopant present in the mixture (c_m) [11,18,20], temperature, and the shape anisotropy of the micelles (S_a) [21]. The pitch length is defined as the distance of one full rotation of the director (n), which can be determined in a simple way [22]. This feature has an important consequence. In some chiral systems, the pitch length has the same order of magnitude as the wavelength of visible light. Therefore, these systems exhibit interesting optical properties, which has been used in optical applications [23–25], such as Bragg reflection and low-threshold laser emission [26].

The structure and local ordering of the micelles in lyotropic liquid crystals presenting in the three nematic phases were investigated by using complementary experimental techniques [27]. Micelles are piled-up in a pseudo-lamellar structure, with a correlation distance corresponding to about 5 micelles. Let us discuss in more details the pseudo-lamellar structure proposed for the micellar nematic phase. In the usual case of micellar isotropic phase, the small-angle scattering pattern presents a single band, isotropically located around the direction of the incident X-ray beam direction. The scattering pattern of lyotropic nematic mesophases (let us say, in oriented samples) is different [27]. Along one of the directions of the scattering pattern, two bands are present. The spacing distances associated with these bands keep a relation between them of 2:1. The presence of these bands was associated with a lamellar-like structure, named pseudo-lamellar structure, of short- range arrangement. In actual lamellar phase, Bragg peaks

* Corresponding author at: Department of Physics, Federal Technological University of Paraná, Brazil.
E-mail address: oscarsantos@utfpr.edu.br (O.R. Santos).

https://doi.org/10.1016/j.molliq.2021.118097
0167-7322/

are present in the diffraction pattern, maintaining the spacing distances in a relation of ...3:2:1, revealing the stack of the lamellae in a parallel arrangement. In the case of lyotropic nematics, the micelles stack up in a short-range arrangement, giving rise to the pseudo-lamellar structure. These results allowed the proposal of the Intrinsic Biaxial Micelle model (IBM) [1], where micelles are assumed to have, on average, a flattened prolate ellipsoidal (orthorhombic) shape in all of the nematic phases. Orientational fluctuations are responsible for the stabilization of the different uniaxial and biaxial phases. The modifications in these fluctuations are due to changes in the micellar shape anisotropy, driven by the temperature. This model has been used in the study of nematic phases in different lyotropic mixtures [28].

In 1988, Neto et al. reported a study about the local ordering in lyotropic cholesteric liquid crystals (using X-ray scattering) in systems composed of potassium laurate (*KL*) and sodium decyl sulfate (*SdS*) doped with the chiral molecules d-Octanol (*DOC*) and brucine sulfate hepta-hydrated (*BS*), respectively [29]. It was shown that the existence of large chiral molecules (*BS*) in the pseudo-lamellar structure, probably not directly incorporated to the micelles, modifies the reciprocal-space scattering image of the Ch_C phase compared to that of the usual N_C. The reciprocal-space image of the Ch_C phase, in this case, could be explained by non-correlated local perturbations of the pseudo-lamellar structure.

In recent years, improvements in the analysis of Small-Angle X-ray Scattering (SAXS) data [30–33] allowed the development of more realistic models to investigate the structure and local ordering of complex fluids by the full-curve fitting of the SAXS data. A question that could be investigated by using advanced modeling is the eventual modification in the form factor of the micelles as well as details on the structure factor of the micellar arrangement induced by the presence of a chiral molecule in a lyotropic cholesteric mixture, compared with these factors in the correspondent nematic phase. The basic design of the experiment consists in comparing the scattering intensity as a function of q (the modulus of the reciprocal space momentum transfer vector) of a magnetic-field oriented N_C phase, with the scattering intensity of the correspondent Ch_C phase, unwound and oriented by the magnetic field. The magnetic field orients the director of the N_C phase parallel to it and in the Ch_C phase, the field unwinds the helical structure, and the micelles will be oriented as in the N_C phase. In the present study, we investigate a lyotropic mixture presenting the N_C phase and its correspondent Ch_C phase, where a small amount of the chiral agent brucine sulfate was added. Polarized optical microscopy and laser conoscopy were used to characterize the phases and SAXS provided details on the micelle structure and supramolecular ordering. The lyotropic nematic mixtures were composed of potassium laurate (*KL*)/potassium sulfate (K_2SO_4)/dodecanol (*DDeOH*)/water and the cholesteric phases were obtained from these mixtures, by adding the chiral molecule, brucine sulfate [13].

2. Experimental section

The lyotropic quaternary mixtures of $KL/K_2SO_4/DDeOH/H_2O$, which presented the nematic phases, were prepared with the following composition in relative molar fraction of each component: *KL*, 0.0382; *DDeOH*, 0.0114; H_2O, 0.9433; K_2SO_4, 0.0060 and the cholesteric phase has been obtained by adding a small quantity of a chiral compound, brucine sulphate (BS), 0.0010 [34]. At this concentration, we evaluate that there are about 2 brucine molecules per micelle, as calculated in section E of the Supplementary Material. The textures of the lyotropic phases were investigated by polarized optical microscopy following the usual procedures (Fig. SM2 (a)) [35–37]. The microscope used was a Leitz Orthoplan-Pol with an Instec HS1 hot stage. Small amounts of the mixtures were transferred into rectangular hollow glass capillaries from VitroCom, with 0.2 mm path length, 2 mm width, and 50 mm length. The ends of the capillaries were closed with a photopolymer resin.

For the unambiguous identification of the three lyotropic nematic phases, and their corresponding phase transitions temperatures, the two optical birefringences $\Delta n = n_2 - n_1$ and $\delta n = n_3 - n_2$, were measured as a function of temperature by laser conoscopy [38]. n_1, n_2 and n_3 are the principal refractive indices of the medium along the axes 1, 2 and 3 of the laboratory frame. The laboratory rectangular frame axes are defined as follows: axis 3 is parallel to the laser beam propagation direction, axis 1 is parallel to the magnetic field direction, and axis 2 is perpendicular to them [34]. For this purpose, well-oriented samples in an external magnetic field were used. Samples of the lyotropic mixtures were transferred into optical glass cells 1.0 mm thick. The main components of the setup are: a HeNe laser (λ = 632.8 nm); a Neocera LTC-21 temperature controller, with precision of 0.01 °C; and a Walker Sci. electromagnet to provide a uniform and static magnetic field of $|H|$ = 2.04 kG. In previous works, additional details about the setup, the sample alignment procedure in each phase, and the measurement procedure were described [35,38].

The SAXS data collection and data treatment were described in detail in our previous work, in its Supporting Information [34]. In summary, a laboratory-based SAXS instrument Xeuss 2.0 (Xenocs) with a Pilatus 300 k detector (Dectris) was used. The X-ray beam is generated in a Cu anode microfocus' X-ray source, with wavelength λ = 1.5419 Å. The measurements were taken in transmission geometry at a distance between the sample and the detector of 936 mm. The samples were put into cylindrical glass capillaries of 1.5 mm diameter and then placed in a temperature controlled sample holder. A static magnetic field of about 1 kG was applied to the samples perpendicularly to the X-ray beam propagation direction (Fig. SM2 (b)). The capillary long axis was perpendicular to both the magnetic field and the X-ray beam. For the purposes of this work, the intensity is expressed as a function of the momentum transfer modulus, $q = (4\pi/\lambda)sin\theta$, where 2θ is the scattering angle and λ is the radiation wavelength. The 2D SAXS images were integrated using program FIT2D [39] and a homemade Python software using the *pyFAI* library [40]. For samples with no preferred orientation in the SAXS pattern, the full azimuthal circle was integrated. For samples oriented under magnetic fields with anisotropic SAXS pattern, circular sectors were taken as described later in the text. Scattering data from the buffer were used for the data treatment.

3. SAXS modeling

3.1. Simple peak analysis

As shown in detail in Supplementary Material (SM), it is possible to describe the Bragg-like peaks by using a simple peak function with a linear background. The advantage of this simple approach is to not make any assumptions on the detailed internal structure of the system (as discussed in the next section) and obtain structural parameters. This analysis will be used later for the investigation of the nature of orientational fluctuations of the micelles.

3.2. Advanced SAXS modeling

The IBM model [18] assumes that micelles, in the nematic and cholesteric lyotropic phases, are flattened prolate ellipsoids, sketched as a brick of sides A' (the biggest dimension), B' and C' (the main amphiphilic bilayer dimension). In a recent paper [41],

a description of the core–shell nature of the micelle is presented to analyze SAXS results. The shell contains the amphiphilic polar heads and counter-ions, and the core, the carbonic chains.

The SAXS data of such systems [17,18,20,41] revealed the presence of Bragg-like broad bands (first and second order) in a pseudo-lamellar arrangement. The scattering data that will be analyzed here come from N_C and Ch_C samples oriented by a magnetic field, along axis 1. The X-ray beam is directed along axis 2. The 2D diffraction patterns are recorded in the 1–3 plane. In these experimental conditions, the orientational fluctuations of the micelles are full rotations around axis 1 (defining the orientation of the phase director) and the scattering along axis 3 informs about a mean value of the micellar dimensions B' and C'. Micelles are piled-up in a pseudo-lamellar structure and the structural parameters obtained from the experimental data fitting are related to the micellar form factor and those from the structure factor. In the model, the micelles were described as a core–shell ellipsoid of rotation with dimensions for the core $R_1, R_2 = \epsilon R_1$ and thickness of the shell t, where ϵ is the anisotropy factor (spheres: $\epsilon = 1$, prolate ellipsoid: $\epsilon > 1$, oblate ellipsoid: $\epsilon < 1$). In this way, the long axis A' is $2\epsilon R_1$ and the two other axes B' and C' are simply described as $B' \sim C' = 2R_1$. As will be discussed later, the low resolution of the SAXS data and the intrinsic fluctuation of the micelles did not allow the determination of B' and C'.

The micelles are assumed to pack on a pseudo-lamellar structure. The proximity of the micelles on each plane gives rise to micelle-micelle steric interactions. In the experiments where ferrofluid nanoparticles are used to improve the sample alignment, these particles form large aggregates that are visible at low scattering angles (in the range $q \lesssim 0.06$ Å^{-1}). The presence of this small amount of ferrofluid do not affect the micelles shape, sizes and micellar arrangement (form factor and structure factor). All these effects are combined in order to allow a full scattering-curve fitting. The final expression used to model the scattering intensities $I(q)$ is given by:

$$I_{mod}(q) = SC * I_{mic}(q) * S_{AGG}(q) * S_{HS}(q) * S_{Lam}(q) + Back \quad (1)$$

The details on the mathematical formulation of this expression can be found as supplemental material (SM). The micelle shape is described on the $I_{mic}(q)$ term as a core–shell ellipsoid of revolution with semi axis R_1, anisotropy ϵ, shell thickness t and ratio between the shell and core electron density contrasts $\left(\frac{\Delta\rho_{shell}}{\Delta\rho_{core}}\right)$. These micelles are assumed to have a certain degree of polydispersity in size σ_{R_1}. The ferrofluid aggregates are modeled as a tri-axes ellipsoid with semi axes s_1, s_2 and s_3 in the term $S_{AGG}(q)$. The micelle-micelle steric interactions are modeled as interacting hard spheres $(S_{HS}(q))$ with effective radius R_{HS} and volume fraction η_{HS}. The pseudo-lamellar arrangement of the micelles is included in the structure factor $S_{Lam}(q)$, with periodicity a, correlation length (domain size) D and the correction for Porod invariant c. This pseudo-lamellar structure gives rise to Bragg-like peaks (bands), described by the peak shape factor v and the thermal fluctuations on the planes are given by a Debye–Waller mean square displacement σ_a^2. An overall scale factor SC and a constant background $back$ are also included. From radial integrations (i.e., fixed q), one can obtain plots of the scattered intensity as a function of the azimuthal angle ϕ. An appropriate fitting of this plot (e.g., see SM) can provide order parameters of 2^{nd} and 4^{th} orders, $\langle P2\rangle$ and $\langle P4\rangle$. In all cases, the fits are performed using least-square minimization procedures. The order parameter of 2nd order can be associated with the degree or orientation of the micelles along a given direction [42,43]. The physical meaning of the order parameter of 4th order is not entirely clear, but some authors associate low values of this parameter (either positive or negative) with broader orientational distributions.

4. Results and discussion

4.1. Micelle form factor determination

As mentioned in the previous section and on SM, the micelle shape is described by a core–shell ellipsoid of revolution form factor. The determination of the micelle form factor is crucial for a reliable modeling of the curves and the determination of structure factor parameters. Ideally, one could try to dilute the system until one has only the micelles in solution, without interaction. However, for the present study, it is not possible to dilute the system below 5wt% of solute (wt% represents weight %) because the mixture becomes inhomogeneous. Fig. 1 shows the 2D diffractograms of the 95wt% water-diluted samples, initially in the N_C and Ch_C phases. At this water concentration, the mixtures present at 25 °C isotropic phases. Radial integrations are shown in Fig. SM6, demonstrating that the samples are not oriented inside the capillaries.

Several tests indicated that below this concentration of solute, one has precipitation and phase separation of the system. Interestingly, at 5wt% one still sees effects of the structure factor, but it is much more attenuated than the ones in the original formulation (which is the concentration of the normal case, 57wt% of solute).

The series of dilution composed of 80wt%, 90wt% and 95wt% of water for the samples with and without brucine were investigated. In all cases the mixtures present at 25 °C isotropic phases. Fig. 2 shows the scattering intensity as a function of q of the N_C (Fig. 2) a and Ch_C (Fig. 2b). As one can see, at low q values ($q < 0.15$ Å^{-1}), there is a characteristic band, indicating the presence of ordered structures. It corresponds to large uncorrelated clusters of micelles, still maintaining the pseudo-lamellar ordering. However, for q values larger than 0.2 Å^{-1}, one can hardly see any effect of the structure factor, indicating that at these high-water concentrations, this region is dominated by the particle's form factor. Therefore, as a first step, the region $q > 0.2$ Å^{-1} is model only with the form factor term, $I_{mic}(q)$, allowing the determination of the micelle inner radius, anisotropy and thickness (see SM). A good estimation for the electron density contrast ratio between the shell and the core is $\left(\frac{\Delta\rho_{shell}}{\Delta\rho_{core}}\right) = -0.2$, as discussed in the SM. The fits are shown in Fig. 2(a, b) (dashed lines) for the systems with and without brucine, respectively. The fitting parameters obtained for the micelle form factor are shown in Table 1. Since the values obtained for all concentrations are similar, here we show only one result for each sample.

This procedure provided a reliable determination of the micelle's form factor parameters. Interestingly, within the low resolution the *SAXS* technique, the overall parameters obtained for the systems with and without brucine are similar, which indicated that this molecule does not change the micelle shape and anisotropy. The values for the form factor parameters do not change when the structure factor is introduced in the modeling. As one can see in Fig. 2 (solid lines), it is possible to fit the full curve by using the complete model. The results for the full model are shown in table SMIII. Aside from several structural details, one can see a systematic increase of the periodicity a with the increase of the water content, varying from ~ 67 Å at 85% of water up to ~ 80 Å for 95% of water. The dimensions of the micelles, assuming the model described in the SM of uniaxial prolate ellipsoidal micelles, are for both phases $A' \sim 60$ Å and $E' = (B' + C')/2 \sim 40$ Å. Even though

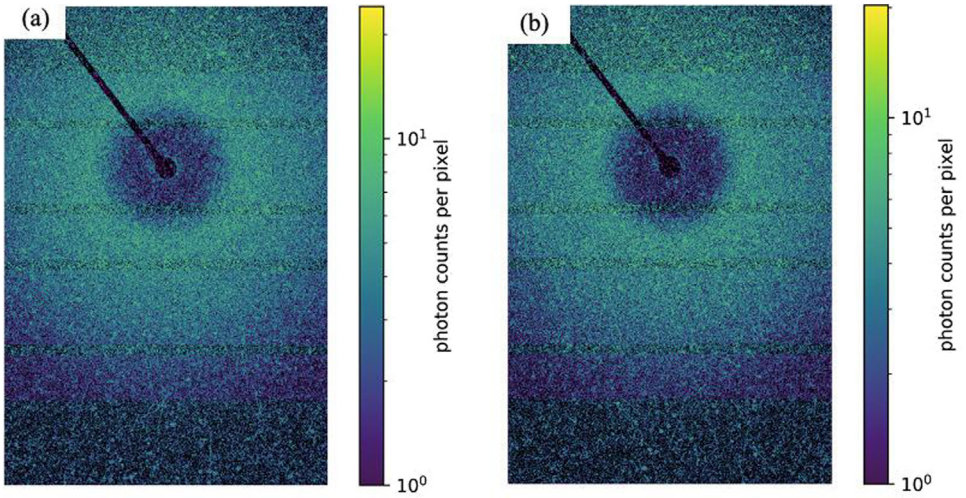

Fig. 1. Typical 2D difractograms of the water-diluted samples (isotropic phase, 95$wt\%$), initially in the N_C (a) and Ch_C (b) phases.

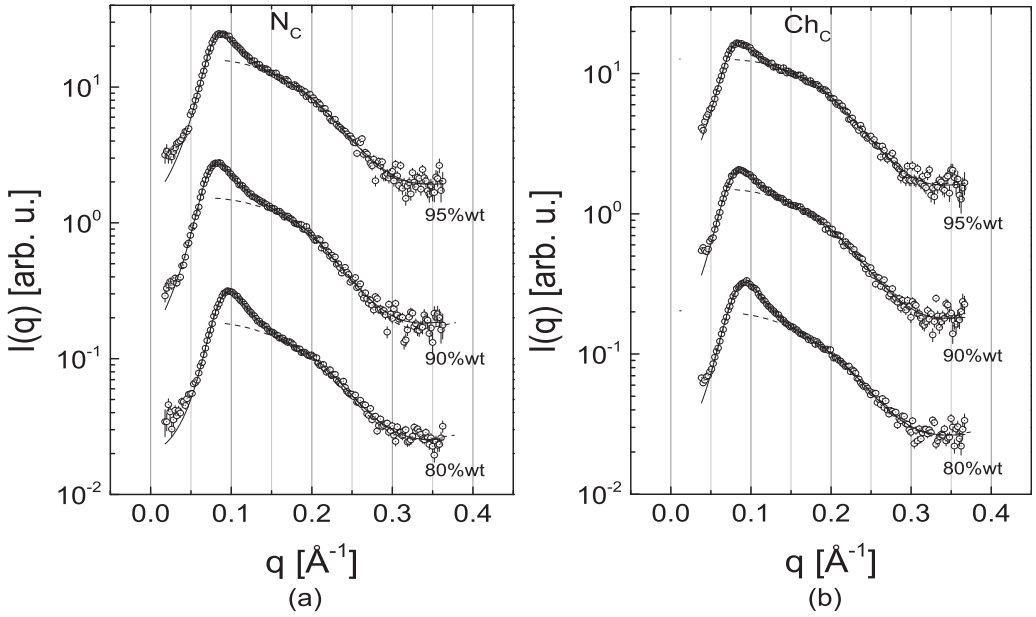

Fig. 2. : Scattered intensity as a function of q of the 95$\omega t\%$ water diluted (a) N_C and (b) Ch_C. Solid lines are model fits of Eq. 2 to the experimental data. The dashed lines are model fits only for the form factor.

Table 1
Model parameters for the form factor.

Parameters (Å)	N_C	Ch_C
R_1	13.1(1)	13.1(1)
t	6.4(2)	6.3(1)
ϵ	1.5(1)	1.5(1)

this modeling was performed for a diluted and non oriented system (isotropic phase), the parameters obtained for the micelles are good initial values for the fit of the scattering data with more concentrated and magnetically oriented samples on the N_C and Ch_C phases [23].

5. Optical characterization

Fig. 3 shows the measurements of the optical birefringences as a function of temperature for the quaternary mixture ($KL/K_2SO_4/DDeOH/H_2O$) in the nematic phase domain. The uniaxial to biaxial transition temperatures were determined from these measurements. After characterizing the nematic phases, the sample was doped with brucine sulfate. One of the characteristics of lyotropic mixtures is the dependence of the temperature phase transitions and even the topology of the partial phase diagrams on the origin and laboratory manipulation of the compounds of the mixture. For example, the KL is usually home-made, from lauric acid. Depending on the steps of this chemical procedure, e.g., number of recrystallizations of the KL, shifts in the transition temperatures may be present when we compare results from the literature. In Ref. [34], the transition temperatures are shifted with respect to those found in the present work. However, the topology of the phase diagram is maintained, with the three nematic phases.

The textures were identified under a polarizing optical microscope. Samples in the N_C phase (Fig. 4a), shows the classical Schlieren texture. When the sample is placed in the presence of a magnetic field ($H = 0.9\ kG$), the director aligns parallel to H, show-

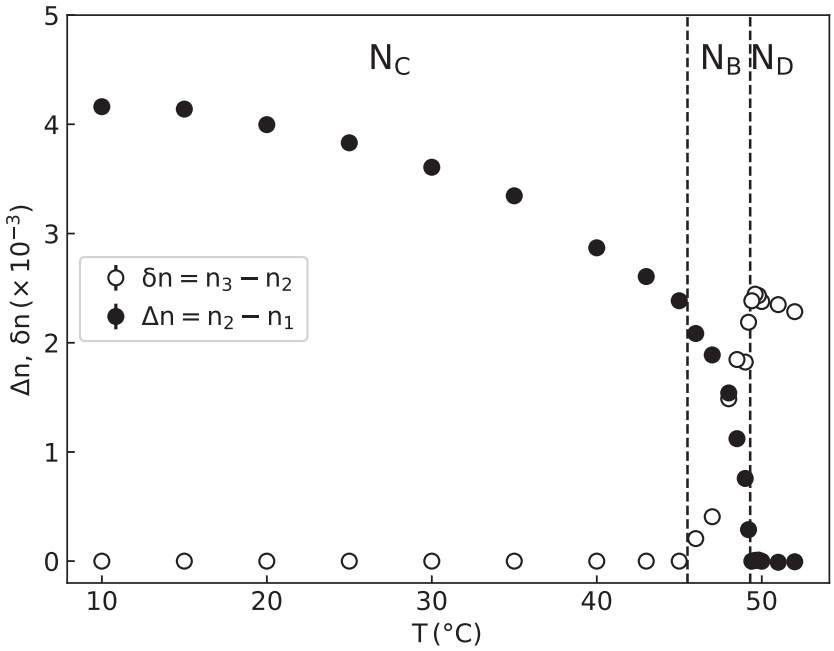

Fig. 3. Temperature dependence of the birefringences, $\Delta n = n_2 - n_1$ (•) and $\delta n = n_3 - n_2$ (○), for the nematic mixture ($KL/K_2SO_4/DDeOH/H_2O$). Obtained through laser conoscopy technique.

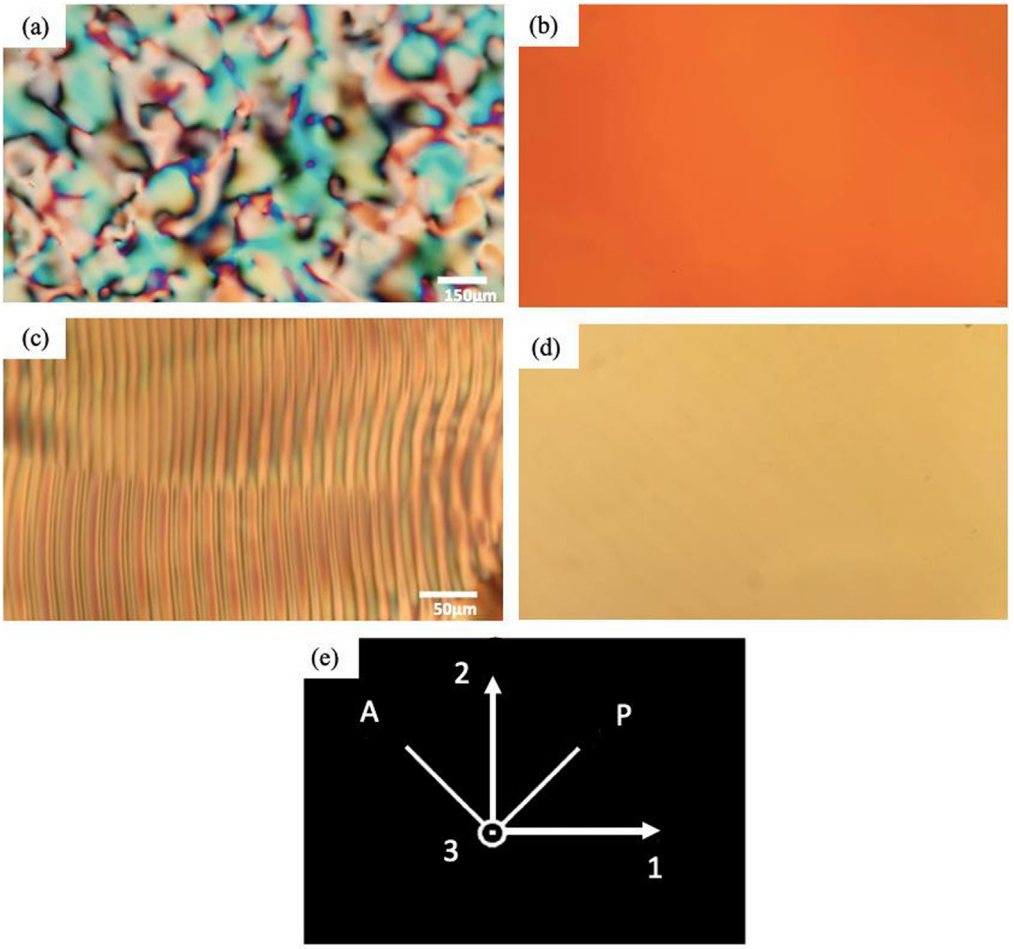

Fig. 4. Lyotropic textures, under a polarizing optical microscope (25 °C), of the: N_C phase without (a) and with (b) the external magnetic field $\vec{H}$; Ch_C phase without (c) and with (d) the magnetic field; (e) *P* and *A* represent the directions of the polarizer and analyzer, respectively. The laboratory frame axes are represented by 1, 2, 3. $\vec{H}$ is oriented along the 1-axis [7,44].

ing a planar texture, characteristic of the N_C phase (Fig. 4b). To obtain the texture showing the twisted Ch_C, we first place the sample in the presence of the magnetic field. Differently from the Ch_B and Ch_D phases, the Ch_C helicoidal structure is unwound by the field (Fig. 4c). In the following, the field is removed and the sample is left at rest for about 36 h and spontaneously the helix is formed, characteristic of Ch_C (Fig. 4d). Fig. 4e represents the laboratory frame axes. The labels *P* and *A* refer to the polarizer and analyzer directions.

6. Structure factor analysis

Fig. 5 shows the typical 2D X-ray diffraction patterns of the N_C (Fig. 5)a and Ch_C (Fig. 5b). Three bands exist in these patterns: two along the 3-axis and one along the 1-axis directions. The outer second-order band along the 3-axis is barely visible in the patterns. Even though the general characteristics of the diffraction patterns of the oriented N_C and Ch_C phases are very similar, a differences in the shape of the strong first-order band can be identified.

Fig. 6 shows the scattered intensity as a function of q along the axes 1 and 3 for the oriented N_C (Fig. 6)a and unwound Ch_C (Fig. 6b). Expression (1) was used to fit the integrated 1D experimental data of $I(q)$ for both samples. Here, the parameters obtained for the form factor of the micelles (Section 5) were inserted in the fit of Eq. (1) as initial parameters, and were left free to be re-adjusted in the fitting procedure. Along the 1-axis direction, we barely identify a shoulder in the $I(q)$ data (Fig. 6). Table 2 gives the fitting parameters obtained in the analysis of the scattered intensity along the 3-axis. As a first remark, the parameters referring to the form factor were, within the errors, the same obtained previously and discussed in Section 5. This result ensures the robustness of the procedure employed to determine the shape and shape anisotropy of the micelles in both mesophases. Moreover, it also supports the conclusion that the micellar form factor, in the present experimental conditions, is not modified by the doping with brucine. However, this may seem contradictory, since now the micelles are oriented under the magnetic field. The similarity among the overall form factor parameters for the oriented and isotropic cases can be explained by the fact that the oriented micelles fluctuate around the magnetic field axis. Therefore, the averaging over the several orientations of the micelles makes it impossible to distinguish the micelle form factors in these two cases.

Let us now focus our attention on the structure-factor parameters a and D obtained from the fits of Eq. (1) to the scattered intensity as a function of q along axis 3. These parameters correspond to the pseudo-lamellar periodicity (a) and correlation length (D) described in SM. The pseudo-lamellar periodicity (the correlation length) is smaller (larger) in the Ch_C phase with respect to this parameter in the N_C phase. The number of micelles in the correlation lengths is about 4 and 5 in the N_C and Ch_C, respectively. These small numbers corroborate the use of pseudo-lamellar for the micellar arrangement, as discussed previously in [27]. The *BS* is a large molecule (about $6.5 \times 10 \times 16\text{Å}^3$) with respect to the micelle size and shows polar regions in different regions of the molecule. Also, taking into account that the sizes of the micelles in both N_C and Ch_C phases remain the same, we expect that the *BS* molecule will be located, mainly, in the water layer between micelles, interacting with the surfaces of adjacent micelles. In other words, the presence of the *BS* between micelles in the Ch_C phase imposes a higher correlation between micelles along the direction of the pseudo-lamellar ordering. It is possible to consider that one molecule of *BS*, having different polar regions on opposite sides of the molecule, could interact with more than one micelle in the pseudo-lamellar structure.

Along the 1-axis direction, there is no indication of the presence even of a short-range positional ordering of the micelles. Actually, it is possible to fit the horizontal cuts with the ellipsoidal core–shell model and a tentative aggregate structure factor. In the fits shown in Table 3, for the horizontal cuts one obtains a radius of ~ 29 Å for the micelle, which corresponds to a maximum diameter of ~ 58 Å . This is remarkably similar to the maximum diameter obtained for the case of randomly oriented micelle indicating that for the horizontal cuts, we are mostly seeing the maximum radius of the oriented micelle.

The order parameter $\langle P2 \rangle$ was calculated from the radial integration of the maximum scattered intensity as a function of the angle ϕ around the 3 axis (see SM). The experimental data and model fits are shown in Fig. SM7 with the obtained parameters shown in Table SM II. From the modeling, the obtained values of $\langle P2 \rangle$ for the phases N_C and Ch_C are 0.8133(6) and 0.747(2), respectively, indicating a slightly higher orientational ordering in the N_C

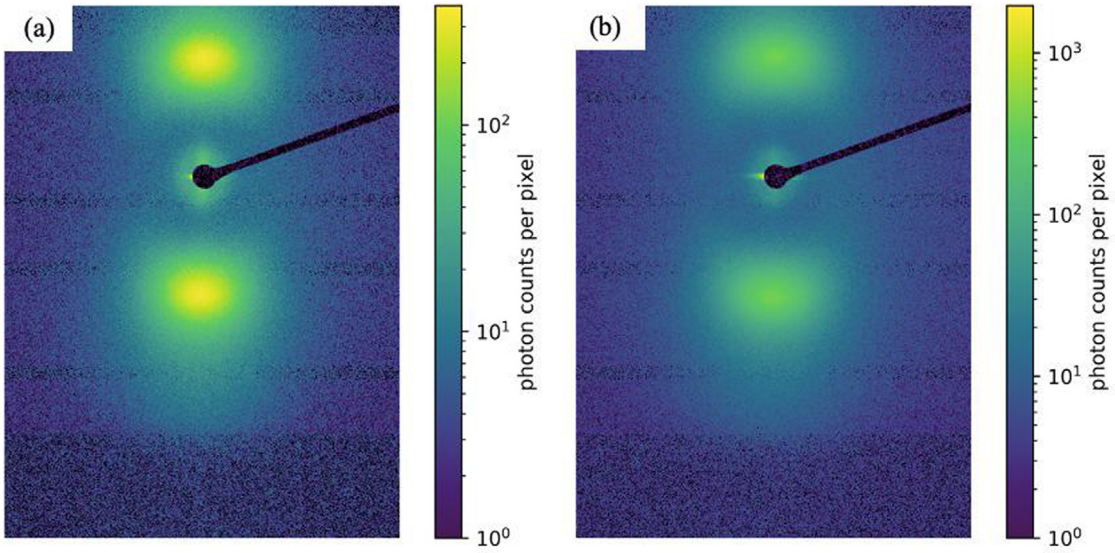

Fig. 5. Typical X-ray diffraction pattern of the N_C (a) and Ch_C (b) phases. The capillary is set up in the vertical direction in the plane of the figure (in the presence of magnetic field). Temperature of 25 °C.

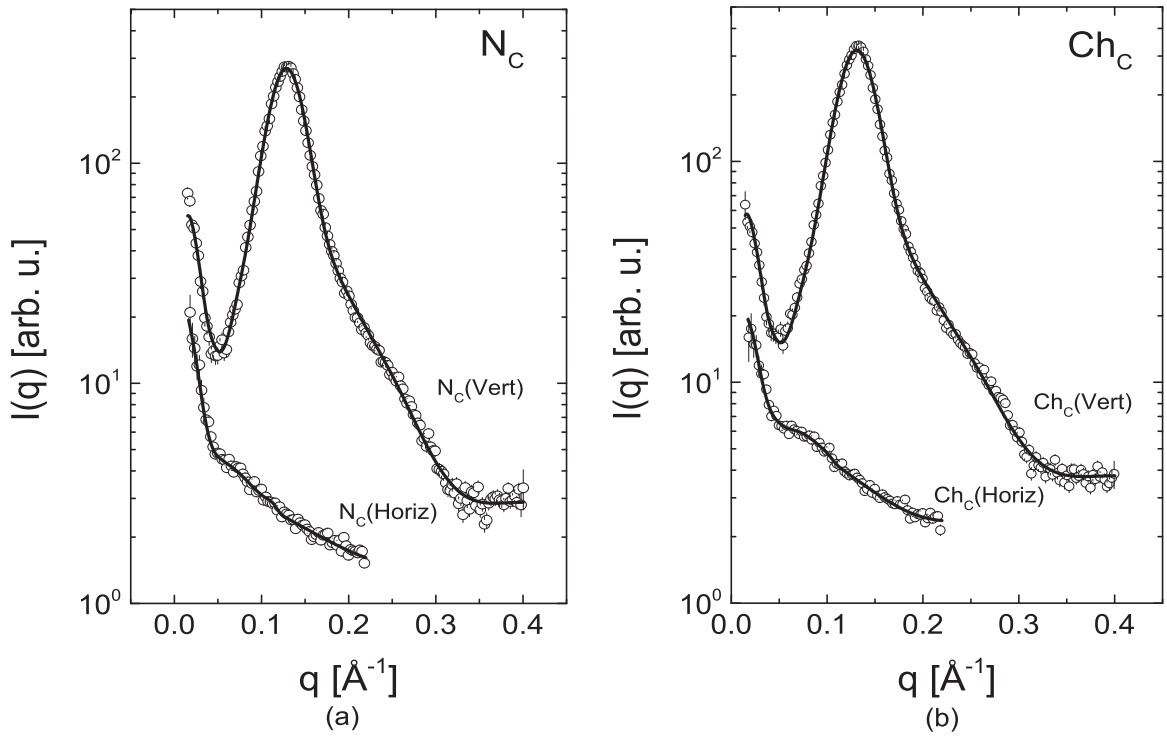

Fig. 6. Scattered intensity as a function of q along the axes 1 and 3 for the oriented. (a) N_C and (b) unwinded Ch_C. Open circles: Experimental data. Solid lines: Model fits.

Table 2
Curve adjustment in the vertical direction of integration.

Parameters (Å)	N_C	Ch_C
R_1	13.0(2)	13.0(2)
t	6.0(3)	6.0(3)
ϵ	1.5(1)	1.5(1)
a	46.0(2)	45.2(2)
D	195(1)	204(1)
$\langle P2 \rangle$	0.8133(6)	0.747(2)
$\langle P4 \rangle$	−0.019(3)	−0.093(5)

Table 3
Curve adjustment in the horizontal direction of integration.

Parameters (Å)	N_C	Ch_C
R_1	22.2(2)	22.0(2)
t	6.6(2)	6.5(2)
ϵ	1.0(1)	1.0(1)
S_1	200(90)	600(100)
S_2	120(9)	100(6)
S_3	66(2)	67(2)
Sc_{agg}	76(40)	134(1)

phase. The values for $\langle P4 \rangle$ for the phases N_C and Ch_C are $-0.019(3)$ and $-0.093(5)$, suggesting a broadening of the angular distributions of the micelles.

From the 2D diffraction patterns, (Fig. SM1) we investigate the shape of the pseudo-lamellar first-order band of both phases. If the maximum of this band spreads along a circumference as a function of the azimuthal angle ϕ, this means that the orientational order parameter is responsible for this behavior. However, if the position of the maximum moves away from a circumference, defects, such as dislocations, are present in the pseudo-lamellar structure [45]. Fig. 7 shows the maximum scattered intensity (obtained varying q at an fixed angle ϕ) as a function of the azimuthal angle ϕ. We observe that, systematically, the results from the N_C phase shows a deviation from the circumference position bigger than that observed in the Ch_C. Associating these deviations to defects (dislocations) in the pseudo-lamellar structure, the presence of the *BS* in between micelles acts to relax part of these defects in the structure. Based on the obtained results it is possible to suggest that, along the 3-axis direction ($\phi = 90°$), micelles are highly correlated. Analyzing this band at higher values of ϕ, this correlation between micelles decreases. As shown in table SMIV we applied the advanced SAXS modeling for the several angles ϕ. The overall results are similar to the above-mentioned analysis, but the use of the advanced model provides structural details for the angular cuts.

7. Conclusion

The small amount of the chiral agent (brucine sulfate) was added in the lyotropic mixture of $KL/K_2SO_4/DDeOH/H_2O$, which presents the N_C phase to obtain its corresponding Ch_C phase. To determine the micelle form factor in both mesophases, we dilute the system with water. Thus, it was identified that for q values larger than 0.2 $Å^{-1}$ one can hardly see any effect of the structure factor, indicating that at these high-water concentrations, this region is dominated by the particle's form factor. The q-region $q > 0.2$ $Å^{-1}$ was modeled only with the form factor term, $I_{mic}(q)$, allowing the evaluation of the micelle dimensions. Assuming the model of uniaxial prolate ellipsoidal micelles, in both phases, the largest axis of the ellipsoid has the dimension $A' = 60$ Å and the mean value of the other two dimensions of the ellipsoid is $E' = 40$ Å. In other words, the micellar form factor, in the present experimental conditions, is not modified by the doping with brucine.

The presence of the *BS* between micelles in the Ch_C phase imposes a higher correlation between micelles along the direction of the pseudo-lamellar ordering. The correlation distances for both phases along the 1-axis direction is about 80 Å and the repeating

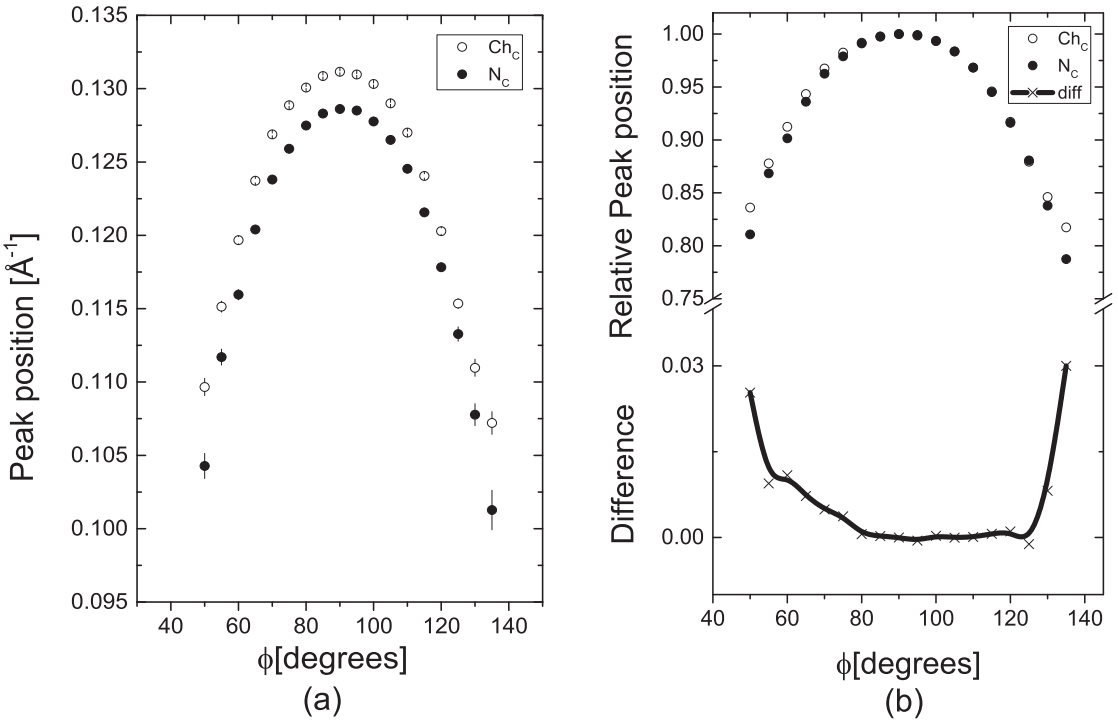

Fig. 7. Position of the maximum scattered intensity I_{max} as a function of the azimuthal angle ϕ. a) position obtained for the two systems. b) positions were normalized by the value at 90°. We clearly see difference at higher angles.

distance is larger than 100 Å, indicating that in the correlation length distance we have less than one micelle. The order parameter $\langle P2 \rangle$ was calculated from the azimuthal integration of the scattered intensity as a function of the angle ϕ around the 3 axis. These values for the phases N_C and Ch_C are 0.8133(6) and 0.747(2), respectively, indicating a slightly higher orientational ordering in the N_C phase. Finally, from the 2D diffraction patterns, we investigate the shape of the pseudo-lamellar first-order band of both phases. We observe that, systematically, the results from the N_C phase shows a deviation from the circumference maximum position bigger than that observed in the Ch_C. Associating these deviations to defects in the pseudo-lamellar structure, the presence of the *BS* in between micelles acts to relax these defects in the structure. The advanced modeling method presented in this work allows the retrieval of structural information of the micelles and their supramolecular arrangements. The method is very flexible and can be used to investigate other types of liquid crystalline systems and arrangements.

Declaration of Competing Interest

The authors declare that they have no known competing financial interests or personal relationships that could have appeared to influence the work reported in this paper.

Acknowledgments

INCT/CNPq (Conselho Nacional de Desenvolvimento Científico e Tecnológico; Grant No.: 465259/2014-6), INCT/FAPESP (Fundação de Amparo à Pesquisa do Estado de São Paulo; Grant No.: 14/50983-3), INCT/CAPES (Coordenação de Aperfeiçoamento de Pessoal de Nível Superior; Grant No.: 88887.136373/2017-00), FAPESP (Thematic Project; Grant 2016/24531-3), INCT-FCx (Instituto Nacional de Ciência e Tecnologia de Fluidos Complexos), and CNPq Scholarships - Brazil (169199/2018-5 and 303001/2019-4).

Appendix A. Supplementary material

Supplementary data associated with this article can be found, in the online version, at https://doi.org/10.1016/j.molliq.2021.118097.

References

[1] A.M. Figueiredo Neto, S.R.A. Salinas, The physics of lyotropic liquid crystals, Oxford University Press, Oxford, 2005, https://doi.org/10.1093/acprof:oso/9780198525509.001.0001.
[2] K. Radley, L.W. Reeves, A.S. Tracey, Effect of counterion substitution on the type and nature of nematic lyotropic phases from nuclear magnetic resonance studies, J. Phys. Chem. 80 (2) (1976) 174–182.
[3] F.Y. Fujiwara, L.W. Reeves, Mesophase behavior and structure of type I lyotropic, J. Phys. Chem. 84 (6) (1980) 653–661, https://doi.org/10.1021/j100443a018.
[4] L.J. Yu, A. Saupe, Observation of a biaxail nematic phase in potassium laurate - 1-decanol - water mixtures, Phys. Rev. Lett. 45 (12) (1980) 1000–1002, https://doi.org/10.1103/PhysRevLett.45.1000.
[5] A.J. Palangana, M. Simões, O.R. dos Santos, F.S. Alves, Periodic structures in a biaxial nematic phase, Phys. Rev. E. 67 (2003) 030701, https://doi.org/10.1103/PhysRevE.67.030701.
[6] W.S. Braga, O.R. Santos, A.R. Sampaio, N.M. Kimura, M. Simões, A.J. Palangana, An optical conoscopy study of a reentrant discotic nematic-biaxial nematic phase transition, J. Mol. Liq. 170 (2012) 72–75, https://doi.org/10.1080/01411594.2021.1945598.
[7] W.S. Braga, O.R. Santos, D.D. Luders, A.R. Sampaio, N.M. Kimura, M. Simões, A.J. Palangana, Conoscopic image of a biaxial negative nematic phase in a potassium laurate-decanol-D_2O mixture, J. Mol. Liq. 187 (2013) 20–23, https://doi.org/10.1016/j.molliq.2013.05.002.
[8] O.R. Santos, W.S. Braga, N.M. Kimura, A.J. Palangana, L.Q. Amaral, Uniaxial and biaxial nematic phases in sodium dodecyl sulphate - decanol - D_2O mixtures, An Optical Conoscopy Study, Mol. Cryst. Liq. Cryst. 615 (2015) 19–25, https://doi.org/10.1080/15421406.2015.1068466.
[9] P.K. Mukerjee, K. Sen, On a new topology in the phase diagram of biaxial nematic liquid crystals, J. Chem. Phys. 130 (2009) 141101, https://doi.org/10.1063/1.3117925.
[10] K. Radley, A. Saupe, Cholesteric states of micellar solutions, Mol. Phys. 35 (5) (1978) 1405–1412, https://doi.org/10.1080/00268977800101051.
[11] L.J. Yu, A. Saupe, Liquid crystalline phases of the sodium decylsulfate/decanol/water system. Nematic-nematic and cholesteric-cholesteric phase transitions, J. Am. Chem. Soc. 102 (15) (1980) 4879–4884, https://doi.org/10.1021/ja00535a006.

[12] B.J. Forrest, L.W. Reeves, M.R. Vist, A type I aqueous cholesteric lyomesophase, J. Am. Chem. Soc. 103 (1981) 690–691, https://doi.org/10.1021/ja00393a042.
[13] D. Reis, E. Akpinar, A.M. Figueiredo Neto, Effect of alkyl chain length of alcohols on cholesteric uniaxial to cholesteric biaxial phase transitions in a potassium laurate/alcohol/potassium sulfate/water/brucine lyotropic mixture: evidence of a first-order phase transition, J. Phys. Chem. B. 117 (3) (2013) 942–948, https://doi.org/10.1021/jp310981d.
[14] E. Akpinar, F. Giesselmann, M. Acimis, Contributions of intermicellar distance, micelle volume and screw angle to the temperature dependence of helical pitch in the intrinsic lyotropic cholesteric phases, J. Mol. Liq. 191 (2014) 20–28, https://doi.org/10.1016/j.molliq.2013.11.024.
[15] E. Akpinar, S. Yurdakul, A.M. Figueiredo Neto, omparison between lyotropic cholesteric phase behavior with partly fluorinated surfactants and their exact hydrogenated counterparts, J. Mol. Liq. 259 (2018) 239–248, https://doi.org/10.1016/j.molliq.2018.03.031.
[16] I. Dierking, F. Giebelmann, P. Zugenmaier, An optical method for the determination of the cholesteric pitch in liquid crystals, Z. Naturforsch. 50a (1995) 589–594.
[17] A.M. Figueiredo Neto, Y. Galerne, L. Liebert, Cholesterization of a biaxial nematic lyomesophase studied by x-ray diffraction and optical microscopy, J. Phys. Chem. 89 (18) (1985) 3939–3941, https://doi.org/10.1021/j100264a036.
[18] A.M. Figueiredo Neto, Micellar cholesteric lyotropic liquid crystals, Liq. Cryst. Rev. 2 (1) (2014) 47–59, https://doi.org/10.1080/21680396.2014.938783.
[19] D.D. Luders, G.A. Zoner, O.R. Santos, W.S. Braga, A.R. Sampaio, N.M. Kimura, A.J. Palangana, M. Simões, An image processing study of a reentrant discotic cholesteric - biaxial cholesteric phase transition, Phase Transitions. 91 (4) (2018) 398–405, https://doi.org/10.1080/01411594.2017.1403606.
[20] A.M. Figueiredo Neto, L. Liebert, A.M. Levelut, Study of ferrocholesteric discotic and calamitic lyotropics by optical microscopy and X-ray diffraction, J. Phys. (Paris). 45 (1984) 1505–1512, https://doi.org/10.1051/jphys:019840045090150500.
[21] M.C. Valente Lopes, A.M. Figueiredo Neto, Influence of the microscopic shape anisotropy of the micelles on the pitch in a cholesteric lyotropic liquid crystal, Phys. Rev. A. 38 (1988) 1101–1104, https://doi.org/10.1103/PhysRevA.38.1101.
[22] G. Arcolezi, D.D. Luders, A.R. Sampaio, M. Simões, W.S. Braga, O.R. Santos, A.J. Palangana, N.M. Kimura, Computational method to determine the pitch length in cholesteric liquid crystals, J. Mol. Liq. 298 (2020) 11752, https://doi.org/10.1016/j.molliq.2019.111752.
[23] P. Palffy-Muhoray, W. Cao, M. Moreira, B. Taheri, A. Munoz, Photonics and lasing in liquid crystal materials, Phil. Trans. R. Soc. A. 364 (1847) (2006) 2747–2761, https://doi.org/10.1098/rsta.2006.1851.
[24] J. Schmidtke, S. Kniesel, H. Finkelmann, Probing the Photonic Properties of a Cholesteric Elastomer under Biaxial Stress, Macromol. 38 (4) (2005) 1357–1363, https://doi.org/10.1021/ma0487655.
[25] P. Yeh, C. Gu, Optics of Liquid Crystal Displays, Wiley, New York, 1999.
[26] V.I. Kopp, B. Fan, H.K.M. Vithana, A.Z. Genack, Low-threshold lasing at the edge of a photonic stop band in cholesteric liquid crystals, Optics Lett. 23 (21) (1998) 1707–1709, https://doi.org/10.1364/OL.23.001707.
[27] A.M. Figueiredo Neto, Y. Galerne, A.M. Levelut, L. Liebert, Pseudo-Lamellar Ordering In Uniaxial And Biaxial Lyotropic Nematics: A Synchrotron X-Ray Diffraction Experiment, J. Physique Lett. 46 (6) (1985) 499–505, https://doi.org/10.1051/jphyslet:019850046011049900.
[28] E. Akpinar, A.M. Figueiredo Neto, Experimental Conditions for the Stabilization of the Lyotropic Biaxial Nematic Mesophas, Crystals 9 (3) (2019) 2073–4352, https://doi.org/10.3390/cryst9030158.
[29] A.M. Figueiredo Neto, A.M. Levelut, Y. Galerne, L. Liebert, Local ordering in lyotropic cholesteric liquid crystals studied by X-ray scattering, J. Phys. France. 49 (1988) 1301–1306, https://doi.org/10.1051/jphys:019880049070130100.
[30] P. Garcia, O. Prymak, V. Grasmik, K. Pappert, W. Wlysses, L. Otubo, M. Epple, C. Oliveira, An in situ SAXS investigation of the formation of silver nanoparticles and bimetallic silver-gold nanoparticles in controlled wet-chemical reduction synthesis, Nanoscale Adv. 2 (1) (2020) 225–238, https://doi.org/10.1039/C9NA00569B.
[31] Y. Sun, P.L.O. Filho, J. C Bozelli Jr, J. Carvalho, S. Schreier, C.L.P. Oliveira, Unfolding and folding pathway of lysozyme induced by sodium dodecyl sulfate, Soft Matter. 11 (39) (2015) 7769–7777, https://doi.org/10.1039/C5SM01231G.
[32] C.L.P. Oliveira, A.M. Monteiro, A.M. Figueiredo Neto, Structural Modifications and Clustering of Low-Density Lipoproteins in Solution Induced by Heating, Braz. J. Phys. 44 (6) (2014) 753–764, https://doi.org/10.1007/s13538-014-0273-z.
[33] S. Forster, A. Timmann, M. Konrad, C. Schellbach, A. Meyer, S.S. Funari, P. Mulvaney, R. Knott, Scattering curves of ordered mesoscopic materials, J. Phys. Chem. B. 109 (4) (2005) 1347–1360, https://doi.org/10.1021/jp0467494.
[34] E. Akpinar, D. Reis, A.M. Figueiredo Neto, Effect of alkyl chain length of alcohols on nematic uniaxial-to-biaxial phase transitions in a potassium laurate/alcohol/K_2SO_4/water lyotropic mixture, Liq. Cryst. 39 (2012) 881–888, https://doi.org/10.1080/02678292.2012.686637.
[35] E. Akpinar, D. Reis, A.M. Figueiredo Neto, Lyotropic mixture made of potassium laurate/1-undecanol/K_2SO_4/water presenting high birefringences and large biaxial nematic phase domain: A laser conoscopy study, Eur. Phys. J. E: Soft. Matter. Biol. Phys. 35 (2012) 1–9, https://doi.org/10.1140/epje/i2012-12050-9.
[36] O.R. Santos, W.S. Braga, D.D. Luders, N.M. Kimura, M. Simões, A.J. Palangana, Study of optical conoscopy in uniaxial and biaxial nematic lyotropic phases, J. Mol. Liq. 197 (2014) 120–123, https://doi.org/10.1016/j.molliq.2014.05.005.
[37] W.S. Braga, O.R. Santos, D.D. Luders, N.M. Kimura, A.R. Sampaio, M. Simões, A.J. Palangana, Refractive index measurements in uniaxial and biaxial lyotropic nematic phases, J. Mol. Liq. 213 (2016) 186–190, https://doi.org/10.1016/j.molliq.2015.10.058.
[38] Y. Galerne, J.P. Marcerou, Temperature-concentration behaviour of the order parameter in the nematic phases of a lyotropic liquid crystal, J. Phys. France 46 (4) (1985) 589–594, https://doi.org/10.1051/jphys:01985004604058900.
[39] A.P. Hammersley, FIT2D: a multi-purpose data reduction, analysis and visualization program, J. Appl. Cryst. 49 (2016) 646–652, https://doi.org/10.1107/S1600576716000455.
[40] G. Ashiotis, A. Deschildre, Z. Nawaz, J.P. Wright, D. Karkoulis, F.E. Picca, J. Kieffer, The fast azimuthal integration Python library: pyFAI, J. Appl. Cryst. 48 (2015) 510–519, https://doi.org/10.1107/S1600576715004306.
[41] E. Akpinar, G. Topcu, D. Reis, A.M. Figueiredo Neto, Effect of the anionic azo dye Sunset Yellow in lyotropic mixtures with uniaxial and biaxial nematic phases, J. Mol. Liq. 318 (2020) 114010, https://doi.org/10.1016/j.molliq.2020.114010.
[42] D.L.P. Dalmolen, S.J. Picken, A.F. de Jong, W.H. de Jeu, The order parameters $\langle P2\rangle$ and $\langle P4\rangle$ in nematic p-alkyl-p'-cyano-biphenyls: polarized Raman measurements and the influence of molecular association, J. de Physique. 46 (8) (1985) 1443–1449, https://doi.org/10.1051/jphys:019850046080144300.
[43] M.T. Sims, L.C. Abbott, R.M. Richardson, J.W. Goodby, J.N. Moore, Considerations in the determination of orientational order parameters from X-ray scattering experiments, Liq. Cryst. 46 (1) (2019) 11–24, https://doi.org/10.1080/02678292.2018.1455227.
[44] Y. Galerne, J.P. Marcerou, Temperature Behavior of the Order-Parameter Invariants in the Uniaxial and Biaxial Nematic Phases of a Lyotropic Liquid Crystal, Phys. Rev. Lett. 51 (23) (1983) 2109–2111, https://doi.org/10.1103/PhysRevLett.51.2109.
[45] Y. Galerne, A.M. Figueiredo Neto, L. Liebert, Microscopical structure of the uniaxial and biaxial lyotropic nematics, J. Chem. Phys. 87 (3) (1987) 1851–1856, https://doi.org/10.1063/1.453199.